

Physical Bias of Galaxies From Large-Scale Hydrodynamic Simulations

Renyue Cen¹ and Jeremiah P. Ostriker²

Received _____; accepted _____

¹Princeton University Observatory, Princeton University, Princeton, NJ 08544;
cen@astro.princeton.edu

²Princeton University Observatory, Princeton University, Princeton, NJ 08544;
jpo@astro.princeton.edu

ABSTRACT

We analyze a new large-scale ($100h^{-1}\text{Mpc}$) numerical hydrodynamic simulation of the popular ΛCDM cosmological model, including in our treatment dark matter, gas and star-formation, on the basis of standard physical processes. The method, applied with a numerical resolution of $< 200h^{-1}\text{kpc}$ (which is still quite coarse for following individual galaxies, especially in dense regions), attempts to estimate where and when galaxies form. We then compare the smoothed galaxy distribution with the smoothed mass distribution to determine the “bias” defined as $b \equiv (\delta M/M)_{gal}/(\delta M/M)_{total}$ on scales large compared with the code numerical resolution (on the basis of resolution tests given in the appendix of this paper). We find that (holding all variables constant except the quoted one) bias increases with decreasing scale, with increasing galactic age or metallicity and with increasing redshift of observations. At the $8h^{-1}\text{Mpc}$ fiducial comoving scale bias (for bright regions) is 1.35 at $z = 0$ reaching to 3.6 at $z = 3$, both numbers being consistent with extant observations. We also find that $(10 - 20)h^{-1}\text{Mpc}$ voids in the distribution of luminous objects are as observed (i.e., observed voids are not an argument against CDM-like models) and finally that the younger systems should show a colder Hubble flow than do the early type galaxies (a testable proposition). Surprisingly, little evolution is found in the amplitude of the smoothed galaxy-galaxy correlation function (as a function of *comoving* separation). Testing this prediction vs observations will allow a comparison between this work and that of Kauffmann et al. which is based on a different physical modeling method.

Subject headings: Cosmology: large-scale structure of Universe – galaxies: clustering – galaxies: formation – hydrodynamics – stars: formation

1. Introduction

The spatial distribution of galaxies provides the core data on which cosmological theories for the growth of structure are based. Spatial correlations, peculiar velocities, voids, etc. have provided the primary evidence for the growth of structure due to gravitational instabilities. But the theories developed to model this growth of structure largely treat the collisionless dark matter, thought to provide the bulk of the mass density in the universe, rather than the observables, the stellar parts of galaxies. Current estimates would put the ratio of the mass densities of these two components at about ($\Omega_{dm}/\Omega_* \approx 0.3/0.003 \approx$) 100, so the potential fluctuations (except on the smallest scales $\Delta r < 10^4 \text{pc}$) are dominated by dark matter mass fluctuations. To accommodate this dichotomy between observables and computables the concept of “bias”, b , was developed (e.g., Davis et al. 1985) to bridge the gap. Treated at first as – what it was – a convenient way of parameterizing our ignorance, it has developed a life of its own.

A common definition would be based on the relation between the number density of galaxies, N_g , (with, e.g., $|m_V| > |m_{V,0}|$) or the total mass density in galaxies ρ_g and the total mass in a given region, ρ_{tot} , with bias, b_l , in regions smoothed by a top-hat smoothing length l defined by

$$\left\langle \left(\frac{\delta N_g}{N_g} \right)^2 \right\rangle_l \approx \left\langle \left(\frac{\delta \rho_g}{\rho_g} \right)^2 \right\rangle_l \equiv b_l^2 \left\langle \left(\frac{\delta \rho_{tot}}{\rho_{tot}} \right)^2 \right\rangle_l . \quad (1)$$

Here we have explicitly put in the scale dependence, although in primitive treatments bias is sometimes treated as a number. The realization that b_l is both stochastic and scale dependent has grown recently (for discussions of analytic theories of biasing see Scherrer & Weinberg 1997 and Pen 1997), but, of course, this must be the case. Blanton et al. (1999a) have studied our simulations taking a broader perspective and allowing, on the right hand side of equation (1), a dependence on variables other than mass density. We restrict ourselves in the current exercise to the conventional parameterization but examine

how b , defined by second equality in equation (1), may depend on spatial scale, galaxy age and other galactic properties. Our simulations do not have sufficient spatial resolution to identify individual galaxies (except in low density regions where they are adequate), due to a tendency of the present simulation to merge distinct systems in high density regions. But galaxy mass (if not number) is conserved during mergers so the smoothed galaxy density (smoothing scale $500h^{-1}\text{kpc}$) is the variable we compare with the similarly smoothed dark matter density. As this smoothing scale is small compared to the correlation lengths we examine ($> 1h^{-1}\text{Mpc}$) we believe that our numerical resolution is adequate (but far from ideal) for the questions examined. A test, presented in Appendix A, comparing two simulations with length scale resolution differing by a factor of two reassuringly show no difference in bias, on the scales studied, which is greater than statistical error ($\sim 10\%$).

Nature has determined bias, not by providing us with a mathematically convenient functional form but through the physical process of galaxy formation. By most current accounts the bulk of the baryons have not condensed into stellar systems, at the present time with the ratio of gas to stars Ω_b/Ω_* ($\approx 0.04/0.003$) ≥ 10 . Thus, galaxies appear to have formed only under favorable conditions. Both simple physical theory and observations indicate greater formation efficiencies in regions of higher density, where cooling processes were more efficient. In the Galaxy, the observed “Schmidt Law” (Schmidt 1959, also see Kennicutt 1989 for an update) stating that star-formation rates scale roughly as the locally averaged value of ρ_{gas}^2 still seems to have some approximate empirical validity. It is based of course on the physical fact that for the dominant collisionally excited line or continuum cooling processes, the gas cooling rate per unit volume – thought to be the rate limiting step – is proportional to ρ_{gas}^2 .

Cosmological observations would also seem to support such a picture since the void regions are believed to be underdense (from simulations) by a factor of 3 – 5 in total mass

density as compared to the average, but, empirically, these regions have a galaxy density far below this (Peebles 1993) in terms of average galaxy density. Conversely, in the great clusters of galaxies, perhaps 10% of the total baryonic mass is in stellar form, indicating above average efficiency of galaxy formation in these very overdense regions.

One reasonable approach to determining bias is to begin by noting directly that most stellar galaxies live within massive halos. Then, one can compute the distribution of dark matter halos and estimate which of these will contain which type of stellar systems. Much work has been done following this promising track in recent years using either large N-body simulations or combining semi-analytic dark matter treatments with detailed hydrodynamic simulations (Cole et al. 1994; Kauffmann, Nusser & Steinmetz 1997). These analyses have produced results which are consistent with many observations.

However, direct numerical simulations can be made on an *ab initio* basis which combine the physical gasdynamic processes used in the hydrodynamic simulations of Katz, Hernquist, & Weinberg (1992) or Steinmetz (1996) with large scale numerical simulations of dark matter pioneered by Davis, Efstathiou, Frenk and White (Davis et al. 1985; Frenk et al. 1985; White et al. 1987). Such calculations could, in principle, determine “bias” by direct computations. We have attempted to do that in earlier work (Cen & Ostriker 1992, 1993b) but, as is well known, the difficulties and uncertainties are formidable. These are of two kinds: inadequate physical modeling and insufficient numerical resolution.

In the last five years we have made quite significant improvements in both our physical modeling and the numerical resolution that we can achieve. First of all, we have upgraded from the somewhat diffusive aerospace gasdynamics-based Eulerian hydrocode (Cen 1992) to a shock capturing, high order, total variation diminishing (TVD) hydrocode (Ryu et al. 1993). A very important additional ingredient in the new TVD code is an implementation of a new, entropy variable into the conventional TVD scheme (Harten 1983). The true

spatial resolution for a given mesh has increased by a factor about two (Kang et al. 1994) and, unphysical spurious heating is removed, allowing for a much more accurate treatment in lower temperature regions. We have also gained a factor of 2.5 through Moore’s Law (increasing computational power), so that the overall gain is approximately a factor of five from $> 1h^{-1}\text{Mpc}$ to $200h^{-1}\text{kpc}$. In particular, our current simulations have a nominal spatial resolution which is small compared to the typical distance between galaxies (cf. Figure 1), which was not the case earlier, so, while we still are totally unable to say anything about the internal structural properties of galaxies, we should be able to specify galaxy integral properties: we feel that the resolution suffices to determine where and when galaxies of normal range will form, and to determine, locally, the mass density in galaxies while we remain unable to say very much about the number density of galaxies.

Secondly, we have substantially improved the realism of the input physics, aside from a seemingly better cosmological model. First, we have added more, relevant microphysical processes due to elements other than hydrogen and helium. The inclusion affects directly cooling/heating, optical opacity, radiation field and indirectly through complex interplays among these physical processes and gravity. Second, in our galaxy formation algorithm, we now allow not only energy feedback from stars but also matter (including metals) ejection into the IGM. Third, we separately but simultaneously follow the dynamics of metals in the IGM, produced during the feedback processes. The algorithm for identifying regions of star-formation which has remained the same has also been used by other workers making detailed hydrodynamic simulations: Katz, Hernquist, & Weinberg (1992), Katz, Weinberg, & Hernquist (1996), Steinmetz (1996), Gnedin & Ostriker (1997) and Abel & Norman (1998). In a region of sufficient overdensity, if three conditions are *simultaneously* satisfied, we assume that an already existing collapse cannot be reversed and that collapsed objects of some kind (stars, star clusters or molecular clouds) will form. The criteria in detail are

as follows:

$$\begin{aligned}
 a) \quad & \nabla \cdot \vec{v} < 0 \\
 b) \quad & M_{gas} > M_{Jeans} \\
 c) \quad & t_{cooling} < t_{dynamical}
 \end{aligned} \tag{2}$$

If all are estimated to be satisfied within a cell, then a mass in gas is removed from the cell (having gas mass M_g) equal to $\Delta M_g = -M_g \Delta t / t_{dyn}$ in a timestep Δt and put into a collisionless particle of mass $\Delta M_* = -M_g$. That particle is labeled with the time of formation, the metallicity of the gas from which it was made and the density of the cell in which it was made. These “stellar” particles have typical mass of $10^7 M_\odot$ and can be thought of as clusters within which star-formation of essentially coeval stars will occur. They are followed after birth by the same code that tracks the collisionless dark matter particles. We find that (except in high density regions) these particles group themselves into galaxy like objects (cf. Fig 1) which have a total mass, a mean time of formation (with dispersion) and a mean metallicity (with dispersion). Within each “galaxy” of defined mean age there will be stellar particles having a wide range of ages as the computed galaxies (like our own) are assembled over time. Even in high density regions we can smooth over some spatial scale and define spatial fields having “stellar” density, age and metallicity.

The top (large) panel of Figure 1 shows the dark matter density for a random slice of size $100 \times 100 h^{-2} \text{Mpc}^2$ and thickness of three cells ($586 h^{-1} \text{kpc}$). Each small tickmark of the top panel has a size of $6.25 h^{-1} \text{Mpc}$. The three bottom pairs of panels show three galaxy groups in this slice in an enlarged display; two separate panels are shown for each selected group with the top panel showing the galaxy density contour and the bottom panel showing the dark matter density contour. Each small panel has a size of $6.25 \times 6.25 h^{-2} \text{Mpc}^2$ and each tickmark for the bottom panels has a size of $391 h^{-1} \text{kpc}$, corresponding to two cells, which is approximately the resolution of the code (Cen & Ostriker 1999). For Group A

we see that the galaxy particles have grouped themselves into two quite separated galactic lumps, whereas the dark matter contour shows only one major lump. For Group B several galactic lumps with varying mass are seen, which roughly follow the distribution of the dark matter, but the difference between galaxy density and dark matter is noticeable. In Group C the two (out of four) galactic lumps in the middle are clearly separated, while they are embedded in a common halo. Clearly any galaxy pairs that are separated by $1h^{-1}\text{Mpc}$ are resolved by the code. We note the fact that we often see distinct galactic mass objects swimming separately in a common halo. This is not due to differences in numerical resolution between dark matter and galaxy particles: the galaxy particles and dark matter particles are followed with the identical PM code. Rather, this occurs because the galaxy particles formed from gaseous accumulations that had undergone radiative cooling and contraction. In the objects shown as distinct lumps all normal dynamical processes are active including dynamical friction and mergers (which of course are somewhat overestimated).

Considering the substantial improvements in the code it seems worthwhile returning to the problem of bias using new simulations. The combination of the improvements already noted allows an identification of individual galaxies in low density regions. In addition, some new questions can now be addressed. For example, we can now study many problems concerning the distribution of metals, in a self-consistent fashion. In this paper we study the relative distributions of galaxy mass density and total mass density, and their evolution in a cold dark matter model with a cosmological constant (ΛCDM). Some aspects (scale dependence of bias) of this work have been reported on in Blanton et al. (1999a). Here we focus on other observables including dependence on epoch.

The new simulations allow us to address the redshift dependence of this bias, which has also been recently addressed by Katz et al. (1998). We will also examine the dependence

on galaxy mass and metallicity and the bias of other constituents such as uncondensed gas in various temperature ranges. Due to the very considerable cost of these large scale simulations we have only completed the analysis of one currently favored cosmological model. Future work will allow us to compare bias amongst models.

After describing briefly further properties of the computational method and the specific cosmological model considered in §2, we present the results in §3. §3.1 is devoted to galaxy bias at redshift zero, while §3.2 examines the evolution of bias of galaxies with redshift. Finally, our conclusions are summarized in §4. Appendix A presents an examination of the effects of the finite numerical resolution on our results by comparing output of two simulations having spatial resolution differing by a factor of two.

2. Method and Cosmological Model

We model galaxy formation as described earlier. Self-consistently, feedbacks into the IGM from young stars in these galaxy particles are allowed, in three related forms: supernova mechanical energy output, UV photons output and mass ejection from the same supernova explosions.

We adopt a cold dark matter model with a cosmological constant (Λ CDM), close to the Concordance Model of Ostriker & Steinhardt (1995) and the preferred model of Krauss & Turner (1995) with the following parameters: $\Omega = 0.37$, $\Omega_b = 0.049$, $\Omega_\Lambda = 0.63$, $h = 0.70$ and $\sigma_8 = 0.80$. The model also is consistent with that favored by recent type Ia supernova observations (Riess et al. 1998). This model is normalized to both COBE and the observed cluster abundance at zero redshift (Eke et al. 1996). The current age of the universe of this model is 12.7 Gyrs, consistent with recent age constraint from latest globular cluster observations/interpretations (c.f., Salaris, Degl’Innocenti, & Weiss 1997).

The choice of the Hubble constant is in agreement with current observations; it appears that $H_0(obs) = 65 \pm 10 \text{ km/s/Mpc}$ can account for the distribution of the current data from various measurements (see, e.g., Trimble 1997). The choice of $\Omega_b = 0.024h^{-2}$ is consistent with current observations of Tytler, Fan & Burles (1996).

The box size of the primary simulation is $100h^{-1}\text{Mpc}$ and there are 512^3 cells (on a uniform mesh), giving the nominal resolution of $197h^{-1}\text{kpc}$. But actual resolution, as determined by extensive tests (Cen & Ostriker 1998), is approximately of a factor of $1.1 - 1.7$ worse than this, depending on the region in question. There are 256^3 dark matter particles used, with the mass of each particles being $5.3 \times 10^9 h^{-1} \text{ M}_\odot$. The typical galaxy particle has a mass of 10^7 M_\odot . Besides this primary box, which will be used for most of our analysis, we have made a higher resolution run with box size $50h^{-1}\text{Mpc}$, with the same number of cells, which will be used for resolution calibration purposes in Appendix A.

3. Results

3.1. Bias of Galaxies At Redshift Zero

Panel (a) of Figure 2 shows the bias of galaxies for four sets ($4 \times 25\%$ in mass) of galaxies ordered by formation time [$z=(0.0-0.8)$, $(0.8-1.0)$, $(1.0-1.3)$, $(1.3-10.0)$], as well as all galaxies at $z = 0$, as a function of top-hat smoothing radius. All scales depicted are considerably larger than our resolution limit; Appendix A indicates that numerical resolution problems should not be important for the results discussed here. As an important aside we note that 50% of the galaxy mass was formed between redshifts 0.8 and 1.3, with median galaxy formation epoch $z = 1.0$, consistent with Madau’s (1997) analysis of the Hubble deep field.

Since all the particles in a given region are tagged with the epoch of formation, the

mean - mass weighted - age of any region is computable at any time. The two youngest sets of galaxies with formation epochs at $z < 1.0$ (dotted and short-dashed curves) are nearly unbiased at large smoothing lengths, e.g., $r_{TH} \sim 15h^{-1}\text{Mpc}$ (above which the limited box size causes the estimate to be inaccurate) and have a bias of ~ 2.0 at $r_{TH} \sim 1h^{-1}\text{Mpc}$, below which our simulation fails. The next set of galaxies that formed at $z = 1.0 - 1.3$ (long-dashed curve), is more strongly biased than the two youngest sets of galaxies. The oldest galaxies (dot-dashed curve) are most strongly biased with a bias ~ 5.5 at $r_{TH} \sim 1h^{-1}\text{Mpc}$ and are still significantly biased at large scales, e.g. ~ 3.0 at $r_{TH} \sim 10h^{-1}\text{Mpc}$. If we think of ellipticals as being the stellar systems within which most star-formation was completed earliest (cf. Searle & Sargent 1972), they should represent, in our terms, the oldest systems. We know these are very overabundant in the rare rich clusters, i.e., in regions of very high overdensity, and so are strongly biased even on large scales (Kaiser 1984). We note from panel (a) that at the fiducial smoothing scale of $8h^{-1}\text{Mpc}$ the bias for all galaxies is 1.35, give $\sigma_{8,gal} = 1.08$ (for $\sigma_{8,mass} = 0.80$), consistent with the observed value of $\sigma_8 = 1.20 \pm 0.18$ (Loveday et al. 1996) (Note that the observed value of σ_8 is for bright galaxies in the APM survey; this is more appropriate for our comparison because the computed galaxy fluctuation is mass-weighted, thus heavily weighted by the most massive, bright galaxies).

Panel (b) shows directly the auto-correlation functions for the stellar mass density of all galaxies, mass and the stellar mass densities of galaxy subsets ordered by formation redshift; the results are consistent with Panel (a) of Figure 2. To summarize, all types of galaxies as well as all galaxies are biased over matter on all scales with two separate trends: 1) at any epoch older objects are more strongly clustered than are younger ones, and 2) bias decreases with increasing scale. Both trends are consistent with our earlier work (Cen & Ostriker 1992). A question has arisen as to whether antibias occurs in these simulations as it does in some quasi-analytic modeling. The answer is “yes” but for different reasons. In dark matter simulations it is found (Kravtsov & Klypin 1998) that in dense regions halos

will merge, with the expectation that the imbedded galaxies will merge as well, reducing the galaxy number density of galaxies (but not the light in galaxies). This effect occurs as well in our simulations but, as is evident from Figure 1, merger of halos does not necessarily lead to mergers of the dissipational galactic components. We find antibias for young systems in dense regions (Blanton et al. 1999b) for the same reason that star-forming regions are rare in real rich and dense clusters of galaxies: the ambient very hot ($T \sim 10^8$ Kelvin) gas can not cool and thus can not accrete onto dense lumps of collisionless stellar or dark matter. This effect sets in as soon as the strong caustics form in our simulations, and considerably before the final accumulation of virialized clusters.

We also sorted our computed sample into four sets by the metallicity of their first generation stars ($Z/Z_{\odot} = [< -1.69], [-1.69 \rightarrow -1.57], [-1.57 \rightarrow -1.48], [> -1.48]$). The trends are comparable to those seen in Panels (a,b) of Figure 2 in the sense that galactic regions with initial high metallicity are more strongly biased than are those with initial low metallicity and any set of objects has an increasing bias with decreasing scale. This presumably reflects the physical situation that high density regions generally have higher metallicity. However, the trend is substantially weaker than that seen in subsets ordered by their formation time.

In Figure 3 we compare the simulation results with observations. In Panel (a) we select the second oldest quartile of objects and designate it as “elliptical galaxies”, whose correlation function is shown along with the correlation functions of observed elliptical galaxies from two independent redshift surveys. Panel (b) shows the correlation function for the second youngest quartile of objects, which we call “spiral galaxies”; also shown are the correlation functions of observed spiral galaxies from redshift surveys. Finally, in Panel (c) we show the correlation function for the density in all objects and total mass in comparison with observed correlations of all galaxies from three redshift surveys. While the separate

subsets (panels a,b) produce results in good agreement with their observational counterparts in the range of scales where our simulation results are most accurate ($1 - 10h^{-1}\text{Mpc}$), the agreement between observations and simulations for all galaxies are not satisfactory. The likely cause is that, while we are computing the correlation functions of galaxy *mass* density, the observed correlation functions are galaxy number weighted and in high density regions the number density of objects will decrease due to mergers while leaving the mass density in galaxies invariant. More robust is the trend found in our computations that older galaxies tend to cluster more strongly than the average in a fashion which is fully consistent with observations.

Figure 4 shows the void probability function as a function of top-hat sphere radius. The void probability function is defined as the probability of a (top-hat) sphere of the given radius having a density of one-fifth of its corresponding global mean (Weinberg & Cole 1992). We see that the probability of having a void as large as $10h^{-1}\text{Mpc}$ in the mass distribution (dot-dashed curve) is 0.005 (the limited box size of the simulation does not allow a probability < 0.005 to be estimated). This has been highlighted by Peebles (1993) as a potential problem for CDM theories. But the void probabilities for various subsets of galaxies and all galaxies are much larger, at $\sim 0.2 - 0.6$, at $r_{TH} = 10h^{-1}\text{Mpc}$. Here we see that the simulations quite naturally produce a universe which over half of the volume is in voids with radii $> 5h^{-1}\text{Mpc}$, while only about 10% of the dark matter universe is in similar voids. Also shown as symbols are observations from Vogeley et al. (1994) of the CfA survey for volume-limited samples with absolute magnitude less than -19.5 (solid squares) and -20.0 (open squares), respectively (fainter samples are not shown because our simulations are likely to have underproduced a significant number of fainter galaxies). Comparing with observations of Vogeley et al. (1994) we see that the real galaxies are indeed quite “voidy”, consistent with the distribution of our simulated galaxies, but inconsistent with the distribution of mass, implying the necessity of biased galaxy formation. Also consistent

with observations are the common trend that older galaxies are more voidy than younger ones, consistent with the fact that they tend to reside in high density regions like rich clusters of galaxies. In the underdense regions examined in the analyses of voids, our spatial resolution is adequate to identify luminous galaxies.

Figure 5 shows peculiar velocity distribution of galaxy mass at $z = 0$ averaged over a top-hat smoothing scale of $1h^{-1}\text{Mpc}$, a typical group scale. Two things come to notice. First, groups of younger galaxies tend to move more slowly than clusters of older galaxies with the difference of the median values between the youngest quartile and the oldest quartile being approximately 100km/s . Second, averaging over all objects, stellar material tend to move slightly more slowly than does dark matter. The latter is equivalent to a small anti-velocity bias, reflecting the gasdynamic effect, while the former clearly indicates that older galaxies tend to reside in higher density, deeper potential regions than do younger ones. The much larger effect - that the small scale velocity dispersion of spirals is far less than the small scale velocity dispersion of ellipticals - cannot be addressed in this work.

3.2. Redshift Evolution of Bias of Galaxies

Let us now study bias at high redshift. Panel (c) of Figure 2 shows the bias as a function of radius at four different redshifts. It is seen that *bias is a monotonically increasing function of redshift*. Second, *bias is a monotonically decreasing function of scale at any redshift with the rate of change a function of smoothing scale (db/dr_{cm}) being nearly independent of redshift*. We think that the increase of bias with redshift is due primarily to the Kaiser (1984) effect. It has also been found in the simulations of Katz et al. (1998). Rarer and rarer events are required at higher and higher redshifts to produce a galaxy of given mass. Finally, we predict that galaxies should be biased over mass by a factor $3 - 4$ on $\sim 10h^{-1}\text{Mpc}$ scale at $z \sim 3$, in excellent agreement with recent observations of high

redshift galaxies at $z \sim 3$ (Steidel et al. 1998), which show strong concentrations of galaxies in narrow redshift bins and imply a strong bias of approximately the same magnitude. Note that our resolution at redshift $z = 3$ is $\sim 50h^{-1}\text{kpc}$ and $\sim 25h^{-1}\text{kpc}$ in the two simulations

In addition we have plotted the auto-correlation functions for all galaxy mass density and total mass density at various redshifts, as a function of *comoving* separation. We have found that, while the correlation of mass grows with time as predicted by linear theory, the correlation function of galaxy density as a function of *comoving* separation evolves very weakly (due to the countervailing evolution of bias) in the pair separation range $r \geq 2.5h^{-1}\text{Mpc}$. This was also found by Katz et al. (1998) in a higher resolution simulation of a much smaller box ($11.1h^{-1}\text{Mpc}$) which uses the same galaxy identification scheme as we do. Where our simulations overlap at redshift $z = 3$ and separation $r = 2h^{-1}\text{Mpc}$, they obtain $\xi = 0.3$ and we find $\xi = 15.0$. The very significant difference is probably due to the differences in simulation box sizes.

In Figure 6 we address evolution in another way by examining the correlation length of the smoothed (mass-weighted) galaxy density as a function of redshift. Shown for comparison are the dark matter particle-particle (short-dashed curve) and halo-halo (long-dashed curve) correlation lengths. Also shown as symbols and a shaded region are available observations from various sources. When needed, observations are converted to be consistent with the adopted cosmological model. We see that, as expected, the correlation function of mass (dark matter particles) is a monotonically decreasing function of redshift: gravitational instability (Peebles 1980) increases correlation with time. On the other hand, the correlation of halos, selected by identifying all regions (cells) at or above the virial density at each redshift, shows a stronger strength at all redshifts than that of galaxy density. Furthermore, the halo correlation shows an interesting “dip” near $z \sim 0.5$,

in contrast to the galaxy density correlation which shows a weak peak at $z \sim 1.0$. The differences could be explained in part by numerical resolution effect and in part by real physical effects. Relatively larger dark matter particle mass compared to the baryonic mass resolution element in the simulation preferentially biases against identification of less massive halos, thus overestimates the correlation of halos at all redshifts. The other effect is physical. At lower redshift ($z \leq 1.0$) the galaxy formation preferentially avoids rich clusters of galaxies, simply because these sites are (as noted earlier) too hot to permit proper cooling and gravitational instabilities to occur effectively. This explains the opposite trends in the halo and galaxy correlations at $z < 0.5 - 1.0$.

Kauffman et al. (1998) have also recently addressed this question and find a drop in the (comoving) correlation length at $z \sim 0.5$, very similar to what we found for dark matter halos, but contrary to what we found for our smoothed galaxy distribution. Hence their result may be due to the method utilized, which is based on identifying N-body halos within which galaxies are expected to reside rather than attempting a full physical simulation. Thus, our result on the correlation evolution for halos (long-dashed curve in Figure 6) is consistent with both that of Colin et al. (1998) from pure N-body simulations and that of Kauffmann et al. (1994) of gas-added halos in the general trend that the halo correlation decreases from redshift $z \geq 3$ to $z \sim 1$ and then rises towards zero redshift; there is a minimum at $z \sim 1$. We caution that the correlation at high redshift may have been overestimated in our simulation thanks to the limited resolution, which preferentially selects out the most massive halos that are most strongly clustered. This indeed may explain the somewhat stronger correlation found in our simulations than in Colin et al. at $z = 3$. At lower redshift this effect is progressively less significant.

Overall, the fit to observation is reasonably good, with both roughly consistent with being flat in the range $z = 0 - 3$. However, one needs to keep in mind that our computed

correlation functions are weighted by the mass in galaxies not the number. Because of this, one expects to have better agreements between our results and observations which look at all galaxies and do not exclude high density regions, if the cosmological model is right and the physical modeling is appropriate. Indeed, the top open square in Figure 6 of Shepherd et al. (1997) data points, which does not exclude clusters in the sample, agrees much better with our results than the bottom open square with an “x” in the middle which does exclude clusters. The same can be said about data point of Giavalisco et al. (1998; open circle with an “x” in the middle), which has a fainter sample than that of Adelberger et al. (1998; open triangle).

4. Conclusions

We analyze a new physically based large ($100h^{-1}\text{Mpc}$) numerical simulation of a plausible ΛCDM cosmological model to quantify the relation expected between mass density and smoothed galaxy density. The results, while consistent, as far as we know, with existent observations are quite inconsistent with the simplest model, where the ratio of galaxy fluctuations to mass fluctuations is a number, b , called bias. This ratio, in principle, could depend on the physical scale being considered, the age or metallicity of the galaxies being studied or the epoch at which the analysis is made. We find in our simulation that bias increases with decreasing scale, with increasing galactic age or metallicity and with increasing redshift. Looking at the average galaxy mass density at redshift zero our result, $b = 1.35$ is consistent with the observed value 1.50 ± 0.19 (Loveday et al. 1996; the quoted observational value is for bright galaxies in the APM survey, which is appropriate for comparison with our model because the computed galaxy fluctuation is mass-weighted, not number-weighted, thus heavily weighted by the most massive, bright galaxies). All of the proposed dependencies can be tested by comparing to observations and if confirmed, used to

interpret large-scale galactic surveys now underway. The surprising emptiness of voids also follows naturally from this physical treatment. We also predict that, due to an apparent coincidence between opposing trends, the strength of the spatial correlation between pairs of galaxies (as a function of *comoving* separation) should be essentially independent of redshift from $z = 0$ to $z = 3$. Here we differ from the Kauffmann et al. (1998) result, thus providing an opportunity to distinguish between the accuracy of the two methods currently being utilized for computing large-scale structure properties from *ab initio* methods. Lastly we find that the perturbations on the Hubble flow for young (e.g., late type spiral or irregular) galaxies should be less than for early type systems; this is a testable proposition.

Much of the complexity and stochasticity of the reported results is due, we believe, to the fact that the conventional treatments (including this one) are not examining all of the right variables. Blanton et al. (1999a,b) show that galaxy density is a function not just of mass density, but also of potential (or velocity dispersion or temperature) in the region under examination. We will return to this in future work with an analysis of the galaxy data using more appropriate variables.

Discussions with Michael Blanton, Guinevere Kauffmann, Jim Peebles, Michael Strauss and Michael Vogeley are gratefully acknowledged as are comments by a referee which enabled us to substantially clarify our presentation. We thank Michael Vogeley for providing the observations concerning void probability functions and correlation functions from the CfA Survey, Douglas Tucker for providing the correlation function data from Las Campanas Redshift Survey and Jon Loveday for providing the correlation function data from APM Survey. The work is supported in part by grants NAG5-2759 and AST93-18185, ASC97-40300.

A. Effect of Finite Numerical Resolution

It is important to understand how the finite numerical resolution might have affected our computed results. We show in Figure 7 results from both $L = 100h^{-1}\text{Mpc}$ and $L = 50h^{-1}\text{Mpc}$ boxes. We smoothed the galaxy and dark matter density fields by a Gaussian window of the same radius $0.5h^{-1}\text{Mpc}$ in both boxes. Panel (a) of Figure 7 shows the bias (defined by equation 1) from the two boxes and panel (b) shows the square root of the ratio of galaxy correlation function to total matter correlation function. We see that two boxes give comparable results with a maximum difference less than 9% (at $r_{TH} = 1h^{-1}\text{Mpc}$, below which no comparison is made; the oscillations at $r_{sp} > 5h^{-1}\text{Mpc}$ on panel (b) are just noise). We therefore conclude that, for the range of scale of interest $r \geq 1h^{-1}\text{Mpc}$, our finite numerical resolution does not significantly affect the results, at least for the quantities examined in this paper, namely bias of the smoothed galaxy density and correlation function of this same function.

REFERENCES

- Abel, T., Anninos, P., Norman, M.L., & Zhang, Y. 1998, ApJ, 508, 518
- Adelberger, K., Steidel, C.C., Giavalisco, M., Dickinson, M.E., Pettini, M., & Kellogg, M. 1998, preprint, astro-ph/9804236
- Bahcall, N.A. 1988, ARAA, 26, 631
- Blanton, M., Cen, R., Ostriker, J.P., & Strauss, M.A. 1999a, ApJ, 522, 590
- Blanton, M., Cen, R., Ostriker, J.P., Strauss, M.A., & Tegmark, M. 1999b, preprint, astro-ph/9903165
- Carlberg, R.G., et al. , preprint, astro-ph/9805131
- Cen, R. 1992, ApJS, 78, 341
- Cen, R., & Ostriker, J.P. 1992, ApJ, 399, L113
- Cen, R., & Ostriker, J.P. 1993a, ApJ, 417, 404
- Cen, R., & Ostriker, J.P. 1993b, ApJ, 417, 415
- Cen, R., & Ostriker, J.P. 1999, ApJ, in press
- Cen, R., Kang, H., Ostriker, J.P., & Ryu, D. 1995, ApJ, 451, 436
- Cen, R., Phelps, S., Miralda-Escudé, J., & Ostriker, J.P. 1998, ApJ, in press
- Cole, S., Ellis, R., Broadhurst, T., & Colless, M. 1994, MNRAS, 267, 541
- Cole, S., Aragon-Salamanca, Frenk, C.S., Navarro, J., & Zepf, S.E. 1994, MNRAS, 271, 781
- Colin, P., Klypin, A.A., Kravtsov, A.V., & Khokhlov, A.M. 1998, preprint, astro-ph/9809202

- Davis, M., & Peebles, P.J.E. 1983, ApJ, 267, 465
- Davis, M., Efstathiou, G., Frenk, C.S., & White, S.D.M. 1985, ApJ, 292, 371
- Eggen, O.J., Lynden-Bell, D., & Sandage, A.R. 1962, ApJ, 136, 748
- Eke, V.R., Cole, S., & Frenk, C.S. 1996, MNRAS, 282, 263
- Evrard, A.E., Summers, F.J., & Davis, M. 1994, ApJ422, 11
- Ferland, G.J. 1994, preprint
- Frenk, C.S., White, S.D.M., Efstathiou, G., & Davis, M. 1985, Nature, 371, 595
- Giavalisco, M., Steidel, C.C., Adelberger, K.L., Dickinson, M.E., Pettini, M., & Kellogg, M. 1998, preprint, astro-ph/9802318
- Gnedin, N.Y., & Ostriker, J.P. 1997, 486, 581
- Guzzo, L., Strauss, M.A., Fisher, K.B., Giovanelli, R., & Haynes, M.P. 1997, ApJ, 489, 37
- Harten, A. 1983, J. Comp. Phys., 49, 357
- Kaiser, N. 1984, ApJ, 284, L9
- Katz, N., Hernquist, L., & Weinberg, D.H 1992, ApJ, 399, L109
- Katz, N., Hernquist, L., & Weinberg, D.H 1998, preprint, astro-ph/9806257
- Katz, N., Weinberg, D.H., & Hernquist, L. 1996, ApJS, 105, 19
- Kauffmann, G., Nusser, A., & Steinmetz, M. 1997, MNRAS, 286, 795
- Kauffmann, G., Colberg, J.M., Diaferio, A., & White, S.D.M. 1998, preprint, astro-ph/9809168

- Kennicutt, R.C. 1989, ApJ, 344, 685
- Krauss, L., & Turner, M.S. 1995, Gen. Rel. Grav., 27, 1137
- Kravtsov, A., & Klypin, A. 1998, preprint, astro-ph/9812311
- Lin, H. 1995, Ph.D. thesis, Harvard University
- Loveday, J., Maddox, S.J., Efstathiou, G., & Peterson, B.A. 1995, ApJ, 442, 457
- Loveday, J., Efstathiou, G., Maddox, S.J., & Peterson, B.A. 1996, ApJ, 468, 1
- Madau, P., 1997, in AIP Conf. Proc. 393, Star Formation Near and Far, ed. S. S.Holt & G. L. Mundy (New York:AIP), 481
- Ostriker, J.P., & Steinhardt, P. 1995, Nature, 377, 600
- Peeles, P.J.E 1972, Physical Cosmology (Princeton: Princeton University Press)
- Peeles, P.J.E 1980, The Large-Scale Structure of the Universe (Princeton: Princeton University Press)
- Pen, U.-L. 1997, preprint, astro-ph/9711180
- Postman, M., Lauer, T.R., Szapudi, I., & Oegerle, W.e 1998, preprint, astro-ph/9804141
- Raymond, J.C., & Smith, B.W. 1977, ApJS, 35, 419
- Ryu, D., Ostriker, J. P., Kang, H., & Cen, R. 1993, ApJ, 414, 1
- Salaris, M., Degl’Innocenti, S., & Weiss, A. 1997, ApJ, 479, 665
- Scalo, J.M. 1986, Fund. Cosmic Phys., 11, 1
- Schmidt, M. 1959, ApJ, 129, 243

- Scherrer, R.J., & Weinberg, D.H. 1997, preprint, astro-ph
- Serle, L., & Sargent, W.L.W. 1972, ApJ, 173, 25
- Shepherd, C.W., Carlberg, R.G., Yee, H.K.C., & Ellingson, E. 1997, ApJ, 479, 82
- Steidel, C.C., Adelberger, K.L., Dickinson, M., Pettini, M., Giavalisco, M., & Kellogg, M. 1998, ApJ, 492, 428
- Steinmetz, M. 1996, MNRAS, 278, 1005
- Trimble, V. 1997, “The Extragalactic Distance Scale” ed. M. Livio, M. Donahue & N. Panagia, p407
- Tytler, D., Fan, X.-M., & Burles, S. 1996, Nature381, 207
- Weinberg, D.H., & Cole, S. 1992, MNRAS, 259, 652
- Weinberg, D.H., Hernquist, L., & Katz, N. 1997, ApJ, 477, 8
- White, S.D.M., Davis, M., Efstathiou, G., & Frenk, C.S. 1987, Nature, 330, 451
- White, S.D.M., Efstathiou, G., & Frenk, C.S. 1993, MNRAS, 262, 1023
- White, S.D.M., Navarro, J., Evrard, A.E., & Frenk, C.S. 1993, Nature, 366, 429
- Vogeley, M.S. 1993, Ph.D Thesis, Harvard University
- Vogeley, M.S., Geller, M.J., Park, C., & Huchra, J.P. 1994, AJ, 108, 745

Fig. 1.— The top (large) panel shows the dark matter density for a random slice of size $100 \times 100 h^{-2} \text{Mpc}^2$ and thickness of three cells ($586 h^{-1} \text{kpc}$). Each small tickmark of the top panel has a size of $6.25 h^{-1} \text{Mpc}$. The three bottom pairs of panels show three galaxy groups in this slice in an enlarged display; two separate panels are shown for each selected galaxies with the top panel showing the galaxy density contour and the bottom panel showing the dark matter density contour. Each tickmark for the bottom panels has a size of $391 h^{-1} \text{kpc}$, corresponding to two cells, which is approximately the resolution of the code (Cen & Ostriker 1999).

Fig. 2.— Panel (a) shows the bias of galaxies for four sets ($4 \times 25\%$ in mass) of galaxies ordered by formation time [$z=(0.0-0.8)$, $(0.8-1.0)$, $(1.0-1.3)$, $(1.3-10.0)$], as well as all galaxies at $z = 0$. Panel (b) shows the auto-correlation functions for all galaxies, mass, galaxy subsets sorted by formation epoch at zero redshift. Panel (c) shows the bias as a function of radius at four different redshifts. Panel (d) shows the auto-correlation functions at various epochs for all galaxies and mass.

Fig. 3.— Panel (a) shows the auto-correlation function for the early type galaxies from the simulation (long-dashed curve with 1σ errorbars) at zero redshift; the second oldest quartile of galaxies is used here. Also shown in Panel (a) are observations for ellipticals from an analysis of galaxies in the Perseus-Pisces region (solid dots; Guzzo et al. 1997) and from the APM survey (solid triangles with 1σ errorbars; Loveday et al. 1995). Panel (b) shows the auto-correlation function for the late type galaxies from the simulation (dashed curve with 1σ errorbars) at zero redshift; the second youngest quartile of galaxies is shown here. The symbols in Panel (b) are observed correlations of spirals (open circles; Guzzo et al. 1997) in the Perseus-Pisces region and from the APM survey (open triangles with 1σ errorbars; Loveday et al. 1995). Panel (c) shows the auto-correlation function for all galaxies (solid curve) and total mass (dot-dashed curve) at zero redshift. The symbols in Panel (c) are

observed correlation functions of galaxies from various surveys: open squares from the Las Companas Redshift survey (Tucker et al. 1997), filled squares from the APM survey (Loveday et al. 1995) and solid dots from the CfA survey (Vogeley et al. 1993).

Fig. 4.— Figure 4 shows the void probability function as a function of top-hat sphere radius for all mass, all stellar mass and three subsets of stellar mass (25%, 50% and 75% oldest stellar mass). The void probability function is defined the probability of a sphere of the given radius having a density of one-fifth of its corresponding global mean (Weinberg & Cole 1992). Also shown as symbols are observations from Vogeley et al. (1994) of the CfA survey for volume-limited samples with absolute magnitude less than -19.5 (solid squares) and -20.0 (open squares), respectively.

Fig. 5.— Figure 5 shows peculiar velocity distributions of various sets of galaxies and dark matter at $z = 0$ averaged over a top-hat smoothing scale of $1h^{-1}\text{Mpc}$. The vertical lines indicate the respective medians of the various sets of objects.

Fig. 6.— Figure 6 shows the correlation length of all galaxies (mass-weighted) as a function of redshift. Also shown are available observations from various sources: the solid dot is from APM observations (Loveday et al. 1995) and Las Companas Redshift survey (Lin 1995) at redshift zero; the solid square is the Autofib survey by Cole et al. (1994) at $\bar{z} = 0.16$; the open squares are from the Canadian Network for Observational Cosmology cluster survey by Shepherd et al. (1997) where the lower square with an “x” in the middle is from extended field sample and the upper square is when the redshift subsample is considered, at $\bar{z} = 0.37$; the cross-shaded region indicates the result from CNOC2 by Carlberg et al. (1998) at $\bar{z} = 0.0 - 0.7$; the open circle with an “x” in the middle is from Giavalisco et al. (1998) from analysis of Lyman Break Galaxies at $\bar{z} = 3.07$; the open triangle is from Adelberger et al. (1998) from counts-in-cells analysis of Lyman Break Galaxies at $\bar{z} = 3.07$; the filled triangle is from Postman et al. (1998) from an angular correlation analysis based on 710,000

galaxies with $I_{AB} < 24$ from a survey of 4×4 square degree, contiguous sky. Also shown for comparison are the dark matter particle-particle (short-dashed curve) and halo-halo (long-dashed curve) correlation lengths.

Fig. 7.— Panel (a) shows the bias (defined by equation 1) from the two boxes with size $L = (100, 50)h^{-1}\text{Mpc}$ and panel (b) shows the square root of the ratio of galaxy correlation function to total matter correlation function. The galaxy and dark matter density fields in both boxes are smoothed by a Gaussian window of radius $0.5h^{-1}\text{Mpc}$. The errorbars shown are 1σ .

Figure 1

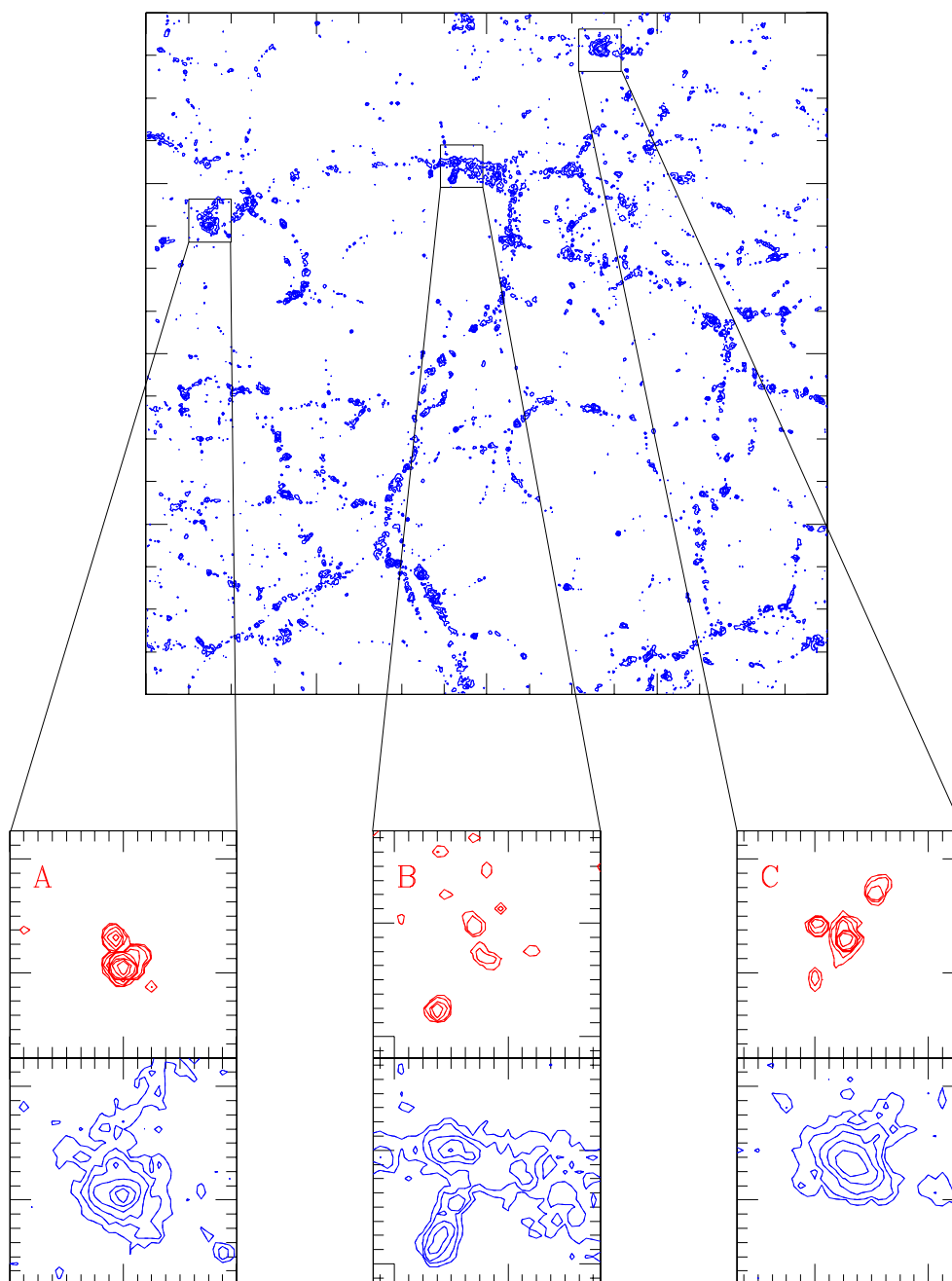


Figure 2

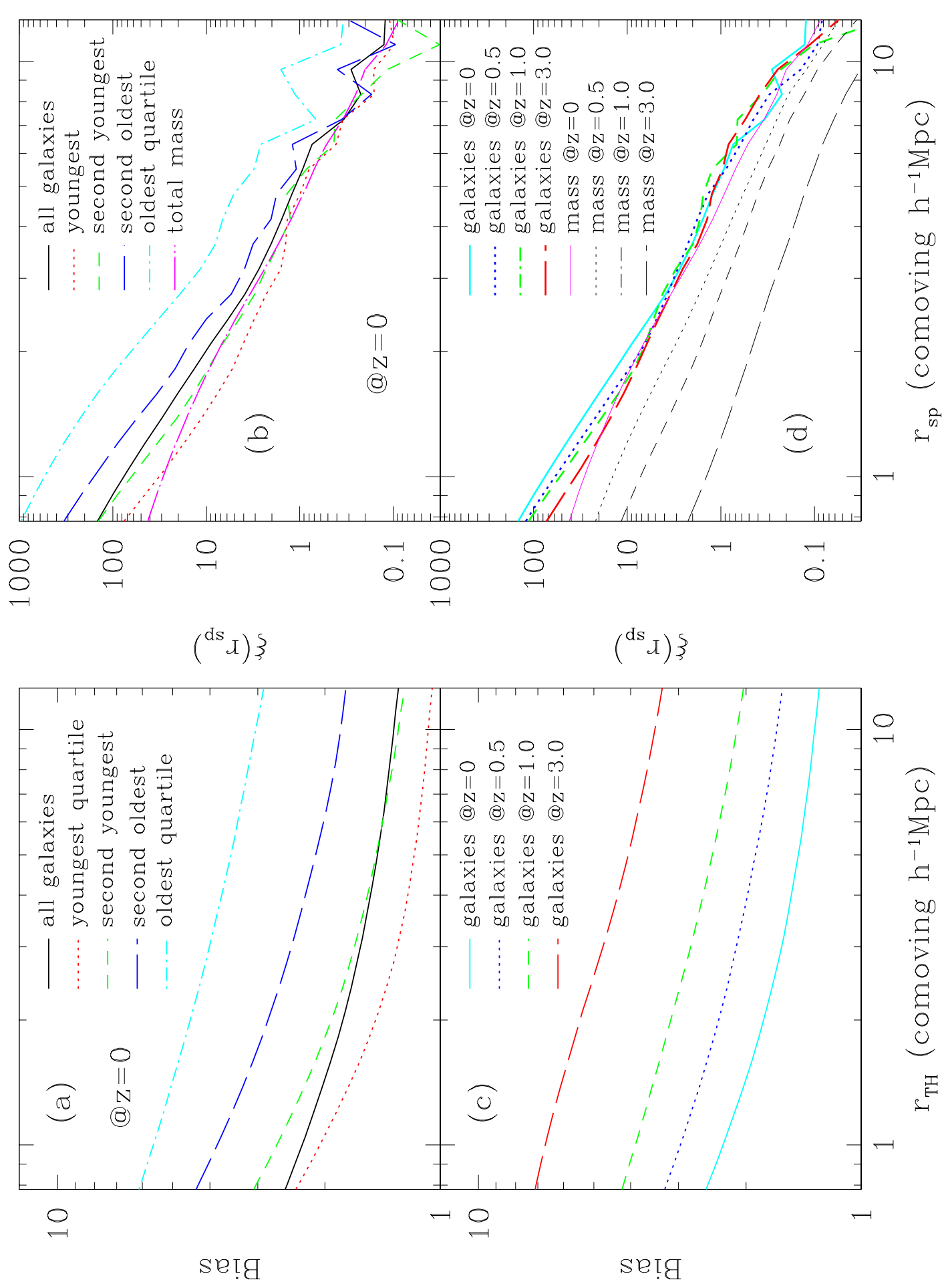


Figure 3

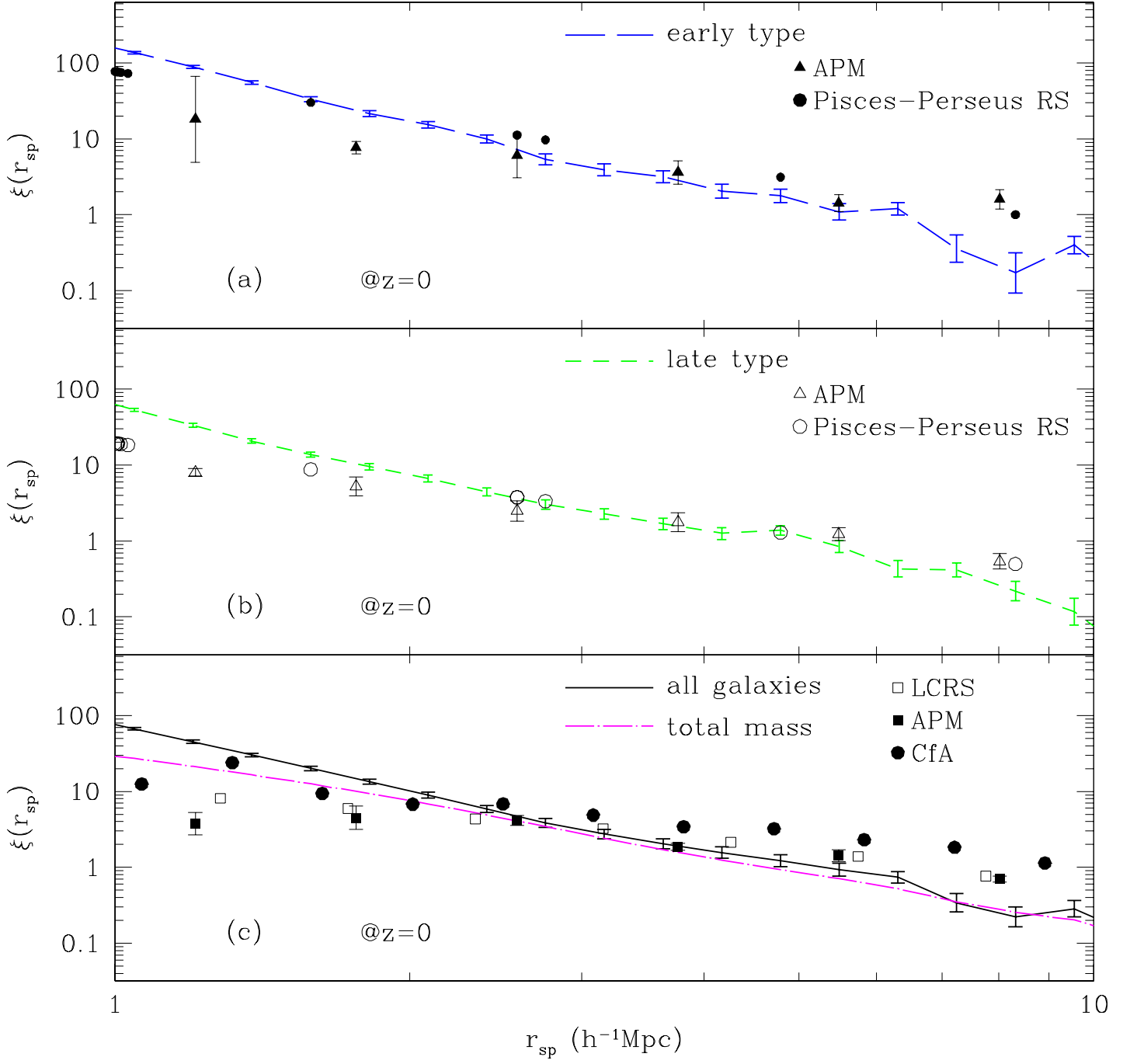


Figure 4

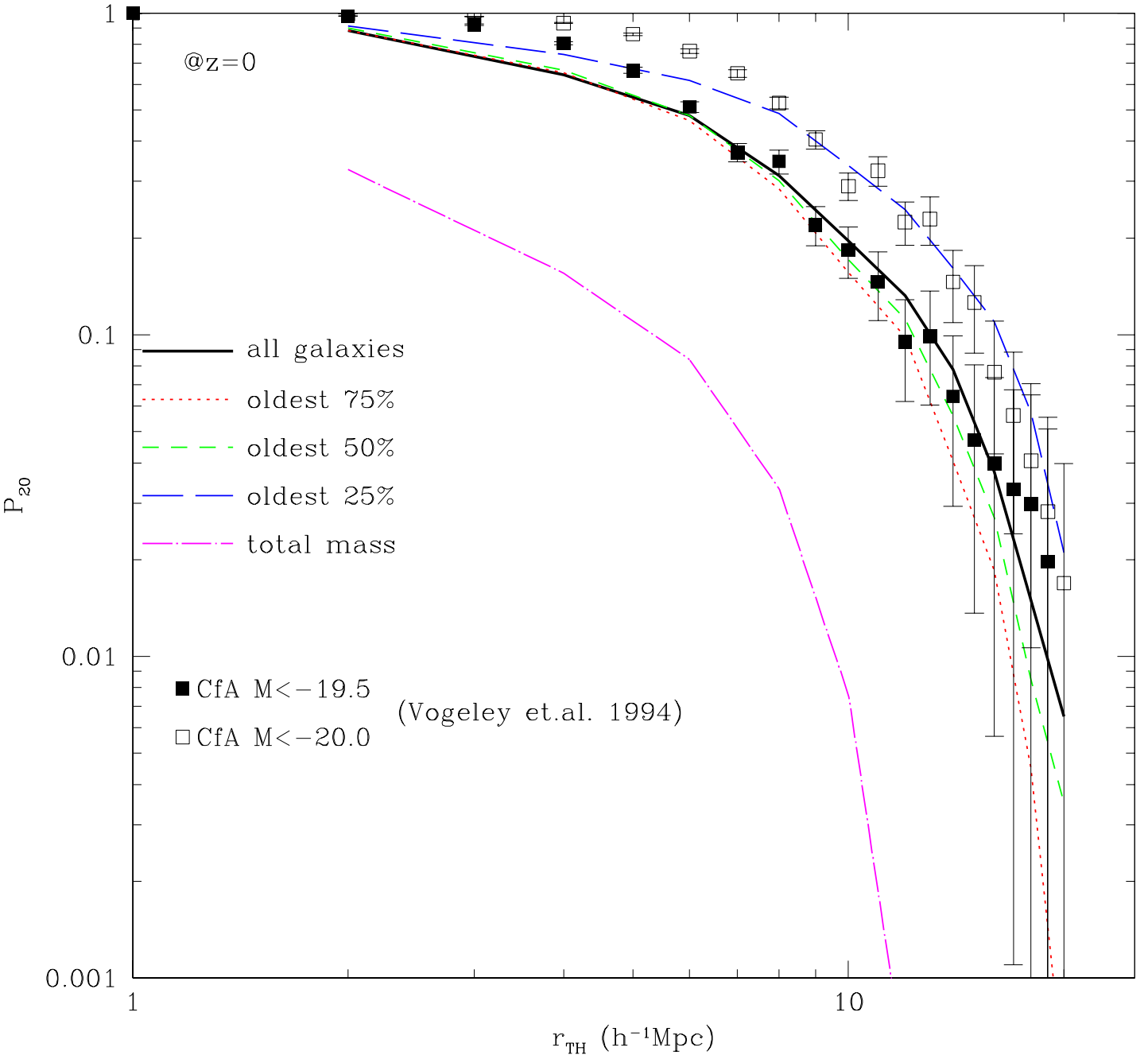


Figure 5

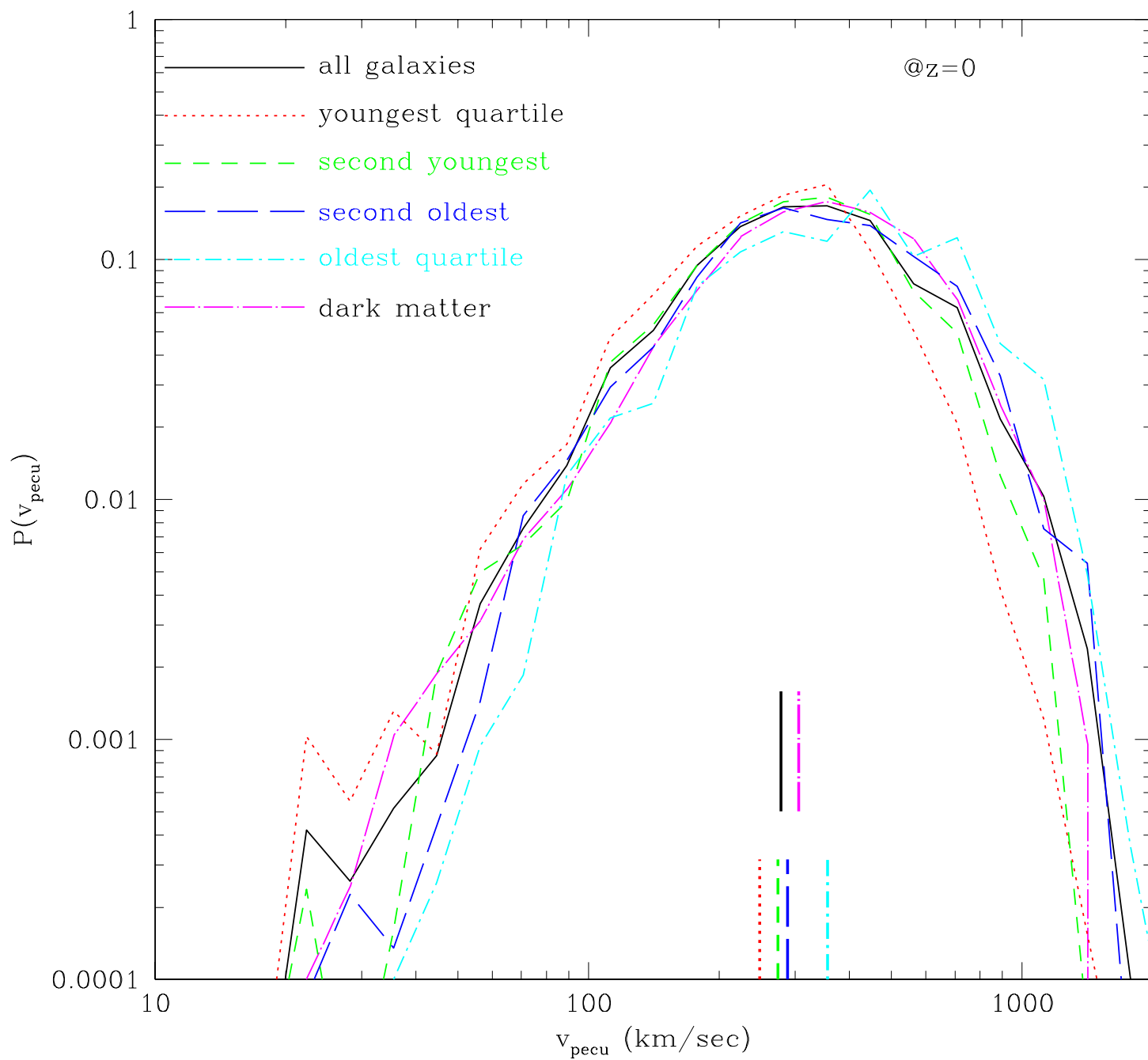
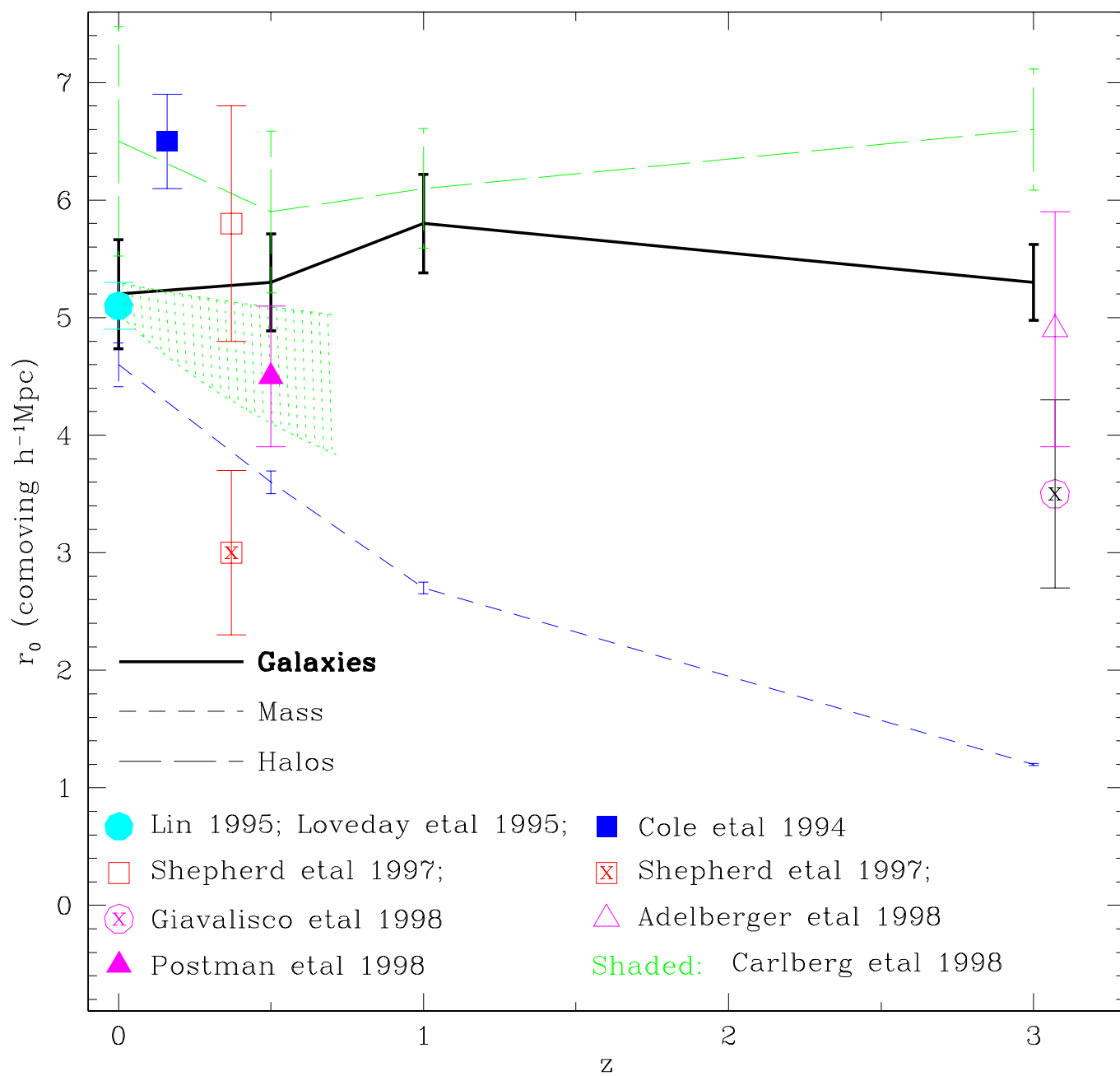


Figure 6



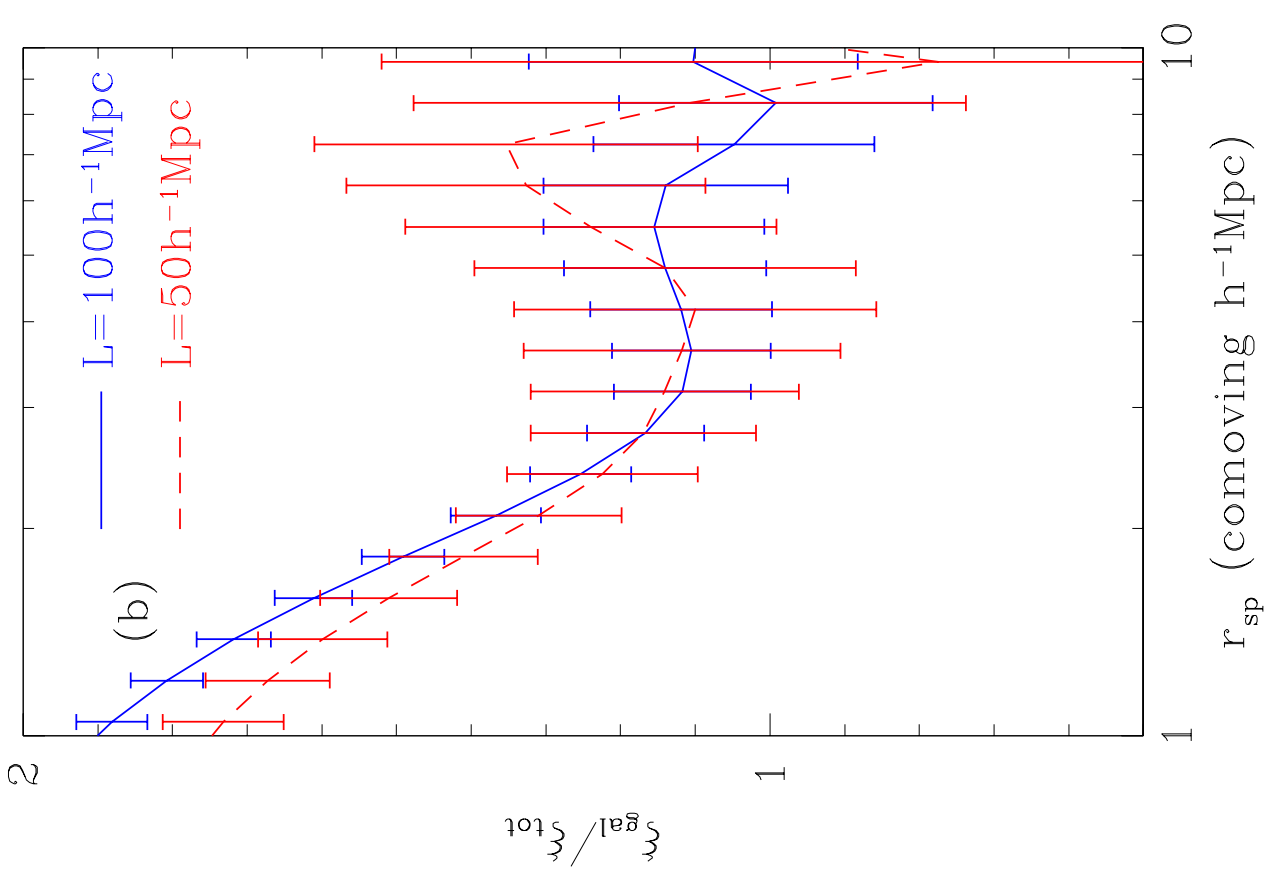
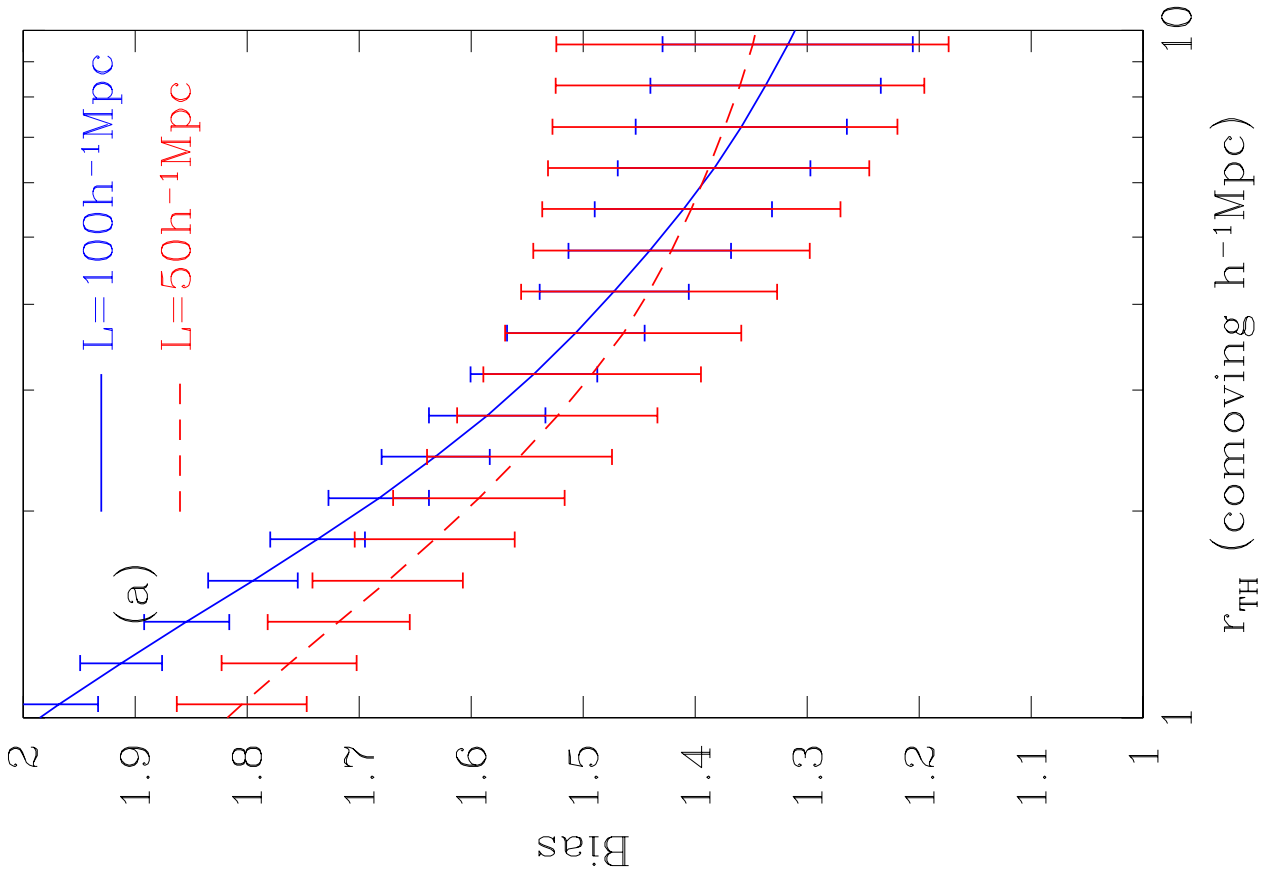


Figure 7